AGU PUBLICATIONS

JGR

Journal of Geophysical Research: Solid Earth

RESEARCH ARTICLE
10.1002/2016JB013653

Key Points:
- We observe an event that we associate with collapse that occurs at approximately 400–600 MPa, in agreement with the literature values. In this region, the sample compresses significantly with little increase in pressure
- At the time of collapse, the differential microscopic stress is approximately 1000 MPa. This value is about an order of magnitude lower than that predicted by a model based on Hertzian fracture mechanics
- We observe a significant number of grains that remain at zero stress, in both axial and transverse directions, even though the mean stress is significantly high at 5.6 GPa. This indicates that vacant pores persist at least to this pressure

Correspondence to:
C. S. N. Cheung,
scheung9@wisc.edu

Citation:
Cheung, C. S. N., D. J. Weidner, L. Li, P. G. Meredith, H. Chen, M. L. Whitaker, and X. Chen (2017), Stress distribution during cold compression of a quartz aggregate using synchrotron X-ray diffraction: Observed yielding, damage, and grain crushing, *J. Geophys. Res. Solid Earth*, *122*, 2724–2735, doi:10.1002/2016JB013653.

Received 15 OCT 2016
Accepted 30 MAR 2017
Accepted article online 3 APR 2017
Published online 22 APR 2017

Stress distribution during cold compression of a quartz aggregate using synchrotron X-ray diffraction: Observed yielding, damage, and grain crushing

C. S. N. Cheung[1,2], D. J. Weidner[1], L. Li[1], P. G. Meredith[3], H. Chen[1], M. L. Whitaker[1], and X. Chen[4]

[1]Mineral Physics Institute, Stony Brook University, Stony Brook, New York, USA, [2]Geological Engineering, University of Wisconsin-Madison, Madison, Wisconsin, USA, [3]Rock and Ice Physics Laboratory, Department of Earth Sciences, University College London, London, UK, [4]Chemistry Department, Stony Brook University, Stony Brook, New York, USA

Abstract We report new experimental results that quantify the stress distribution within a quartz aggregate during pore collapse and grain crushing. The samples were probed with synchrotron X-ray diffraction as they were compressed in a multianvil deformation apparatus at room temperature from low pressure (tens of megapascal) to pressures of a few gigapascal. In such a material, stress is likely to concentrate at grain-to-grain contacts and vanish where grains are bounded by open porosity. Therefore, internal stress is likely to vary significantly from point to point in such an aggregate, and hence, it is important to understand both the heterogeneity and anisotropy of such variation with respect to the externally applied stress. In our quartz aggregate (grain size of ~4 μm), the measured diffraction peaks broaden asymmetrically at low pressure (tens of megapascal), suggesting that open pores are still a dominant characteristic of grain boundaries. In contrast, a reference sample of novaculite (a highly dense quartz polycrystal, grain size of ~6–9 μm) showed virtually no peak broadening with increasing pressure. In the quartz aggregate, we observed significant deviation in the pressure-volume curves in the range of P = 400–600 MPa. We suggest that this marks the onset of grain crushing (generally denoted as P^* in the rock mechanic literature), which is commonly reported to occur in sandstones at pressures of this order, in general agreement with a Hertzian analysis of fracturing at grain contacts.

1. Introduction

Compaction in porous rock is of fundamental importance to reservoir and geotechnical engineering. Any natural phenomena or artificial geological (e.g., oil and gas extraction) application that reduces pore pressure is also likely to cause an increase in the effective stress [*Terzaghi*, 1923]. Such an increase in effective stress may be sufficient to cause inelastic deformation of the reservoir rock in very porous or weakly consolidated reservoirs. In turn, this may lead to production issues, such as surface subsidence, changes in the fluid flow pattern, and permeability of the reservoir. Therefore, a fuller understanding of the compaction process is crucial to predicting both the occurrence and extent of such inelastic deformation.

In typical compaction studies, an axial force is applied across the cross-sectional area of a cylindrical sample by a moving loading ram. The magnitude of the applied stress is then simply calculated by dividing the applied force (measured by using a load cell) by the initial cross-sectional area of the sample. Stress calculated in this way is an average, bulk value and, as such, does not express fully the features of the local stress state within a complex, granular material such as detrital sedimentary rock. For example, what is the microscopic stress distribution? When and at what stress level does the sample yield to close pore space? How do sample properties (such as elastic anisotropy, plastic anisotropy, and grain morphology) affect the compaction process? Detrital sedimentary rocks are naturally formed by aggregation of mineral grains that are compacted and cemented together through depositional and diagenetic processes. Such aggregates inherently contain pores, which are composed of the voids between grains that are present mainly due to inheritance from the geometry of grain packing and secondary dissolution. Therefore, it is expected that any applied load must be supported by grain-to-grain contacts within this structural framework. Hence, stresses are expected to concentrate at the grain-grain contacts and vanish at grain-pore interfaces. There are several additional complicating factors within this general scenario. First, the local stress field will be modified by

inherited microstructural artifacts that are inevitably present within any detrital sedimentary rock, such as diagenetic cement, grain shape, grain packing, and preexisting faults and fractures. Second, even though the average stress applied to the end surfaces of samples is known, the stress distribution within the sample volume under compression is not constrained by this. It is well known that cylindrical samples loaded in the way described above exhibit an *end effect*; a boundary effect whereby the average stress is concentrated near the contact between the sample and the loading rams due to interface friction but varies heterogeneously and anisotropically within the sample interior. For example, *Peng* [1971] demonstrated how strain varied heterogeneously within samples of granite and steel during uniaxial compression under different end conditions.

Our approach to quantifying the internal stress distribution is different. We measure stress indirectly by using the atomic lattice spacing within grains, as revealed by X-ray diffraction, as a measure of local elastic strain. If the whole sample was subjected to a state of uniform hydrostatic stress, then the lattice spacing would change with increasing hydrostatic stress, but would be identical in each grain. Any departure from uniform lattice spacing will therefore be due to local nonhydrostatic or deviatoric stresses. The stress on each grain can be characterized by the three principal stresses and the orientation of the stress tensor. Here the stress is deduced from strains and an appropriate relation between strain and stress. In this study, we measured lattice spacings, and inferred stress distributions, on samples of a quartz aggregate and a novaculite (as end-members of the spectrum of quartz-rich geo-materials) at pressures from a few tens of megapascal up to several gigapascal.

2. Methodology

2.1. Sample Description

We chose to use a quartz aggregate for this study as an end-member of the quartz-bearing geomaterials that are abundant in the crust. Our sample material is prepared by grinding pure quartz (SiO_2) to a mean grain size of ~4 μm, which is optimal for the X-ray diffraction signal. X-ray diffraction spectra of this material confirmed that it is a pure quartz phase (by fitting the peaks with the "Match" program from Crystal Impact). The quartz powder is hand-packed into the cylindrical space (2.06 mm diameter × 2.06 mm long) within a multianvil cell assembly ($6.18 \times 6.18 \times 6.18$ mm^3) to produce the lower halves of our compound test samples. The multianvil cell assembly (Figure 1a) consists of a cube of pyrophyllite or boron epoxy as a pressure medium. Pyrophyllite is used for lower pressures, while boron epoxy is used for higher-pressure conditions. Based on a close-packed grain arrangement, we estimate that the initial porosity of our quartz aggregate samples is about 25%.

Samples of novaculite, with the same sample dimensions, were also prepared and inserted into the upper half of the cylindrical space within the same sample assembly as a reference material for all eight experiments. Novaculite is a low-porosity, natural quartzite and was selected because of its homogeneity and purity. Its appropriateness as a reference material is demonstrated by the observation that its diffraction peaks exactly matched the quartz powder diffraction peaks at zero pressure but, unlike the quartz powder, the novaculite peaks experienced very little broadening with increasing pressure. Our samples (~2.06 mm diameter) were cored from Arkansas novaculite, kindly provided by Prof. Pamela Burnley (University of Nevada Las Vegas (UNLV)). This material has a very low porosity of approximately 1% and a grain size in the range of ~6–9 μm [*Burnley and Zhang*, 2008].

2.2. Compression Using DIA Apparatus

We performed eight compression experiments using the compound sample assembly described above. Of these, seven experiments [experiments SIO2_47-SIO2_51, SIO2_53-SIO2_54] were carried out in the DIA apparatus installed in the press in the X17B2 hutch at the National Synchrotron Light Source I at Brookhaven National Laboratory and one [experiment SIO2_55] in the 6BM-B hutch at the Advanced Photon Source at Argonne National Laboratory (Table 1). The experimental setup at both beamlines consisted of four, X-ray transparent, sintered diamond and two tungsten carbide (top/bottom) anvils to compress a cube-shaped sample assembly. These anvils were driven inward simultaneously by two wedged guide blocks forced together by a 1100 t hydraulic press [*Wang et al.*, 2003]. The stress field was generated by driving these anvils toward the sample. Macroscopic deviatoric stress can occur due to the strength of the

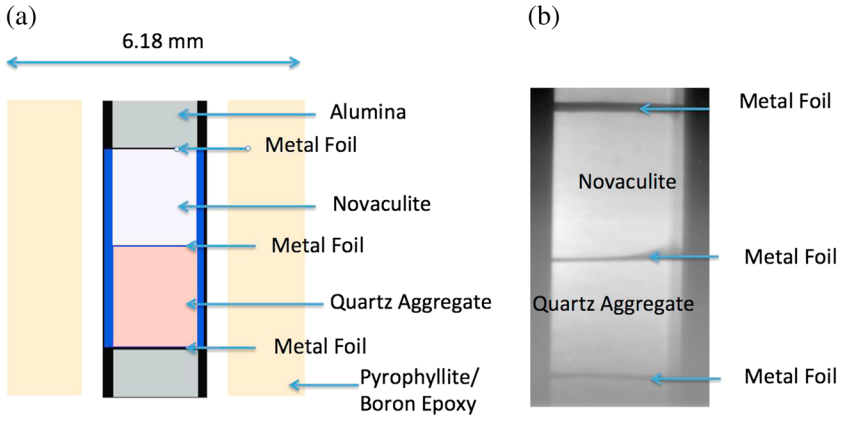

Figure 1. The multianvil cell assembly (6.18 × 6.18 × 6.18 mm^3) consists of a cube of pyrophyllite or boron epoxy as a pressure medium (Figure 1a). A cylindrical space (2.06 mm diameter × 2.06 mm long) in the pressure medium was lined with nested sleeves of metal foils to obtain better contrast for quantifying the sample volume using radiography (Figure 1b). The quartz aggregate and novaculite were hand-packed to produce the top and the lower halves of our compound test samples, respectively.

pressure medium coupled with the cylindrical geometry of the cell assembly, while microscopic deviatoric stress is generated as a result of the heterogeneities and anisotropies within the sample itself.

A horizontal white X-ray beam was projected through the sample assembly, perpendicular to the cylindrical axis of the cell. The X-rays, diffracted by the sample, were measured by using 10 energy dispersive detectors. Nine detectors, separated by 22.5°, formed a semicircular array around the sample. Detector 10 was located on the opposite side of the circle, directly opposite to detector 5. This is illustrated in Figure 2, with only detectors 1, 5, 9, and 10 indicated, which are the detectors on which our analysis is based. Each detector produced a diffraction signal, where the vector normal to the lattice plane is parallel to the diffraction vector. The diffraction vector is defined as the bisector between the incident X-ray and the detector. Detectors 1 and 9 measured diffraction from crystallographic planes whose normal is nearly parallel to the vertical axis. Detectors 5 and 10 measured diffraction from crystallographic planes that are close to a plane defined by the transverse axis. Sets of diffraction patterns were obtained at each collection. A conical slit that sat between the sample and the detectors determined the two-theta angle of the diffracted X-rays (6.5°) and eliminated most of the diffraction diffracted from outside of the sample [*Durham et al.*, 2002]. Since each X-ray detector is highly collimated, and the beam is narrow, the sample volume that contributes to each diffraction pattern is small: about 0.1 × 0.1 × 1.0 mm^3. Hence, the diffraction data focus on a small volume within the solid grains of the quartz aggregate or the novaculite sample.

Each diffraction peak is the sum of diffraction from the relatively small number of grains within this volume that are appropriately oriented for diffraction, as illustrated in Figure 3. These grains (Figure 3) share the characteristic that the normal to the particular diffraction plane (e.g., [101]) bisects the angle between the incident beam and the diffracted beam. Thus, the lattice spacing of each grain or portion of a grain samples the local stress field. If the whole sample is in a state of uniform hydrostatic stress, then each grain will contribute a diffraction signal with identical lattice spacings. If the sample is in a state of uniform axial stress,

Table 1. Eight Experiments Were Performed Under the Following Conditions in the Corresponding Facilities in This Study

Experiment Number	Pressure	Temperature	Time Duration for Each Spectra (s)	Facilities
SIO2_47	ambient to 1.2 GPa	ambient	100	NSLS1/X17B2
SIO2_48	ambient to 1.2 GPa	ambient	100	NSLS1/X17B2
SIO2_49	ambient to 1.2 GPa	ambient	100	NSLS1/X17B2
SIO2_50	ambient to 1.2 GPa	ambient	100	NSLS1/X17B2
SIO2_51	ambient to 1.2 GPa	ambient	100	NSLS1/X17B2
SIO2_53	ambient to 5 GPa	ambient	100	NSLS1/X17B2
SIO2_54	ambient to 5 GPa	ambient	100	NSLS1/X17B2
SIO2_55	ambient to 5.6 GPa	ambient	500	APS/6BM-B

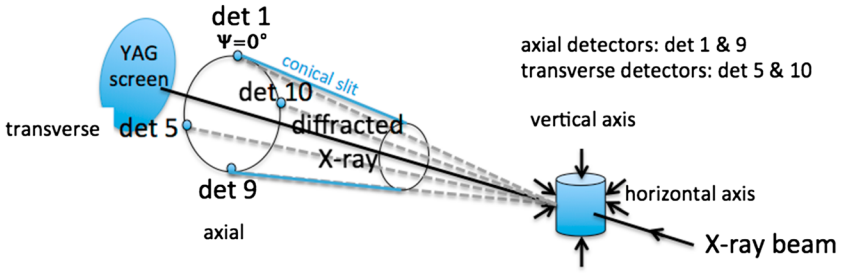

Figure 2. A horizontal white X-ray beam was projected through the sample assembly, perpendicular to the cylindrical axis of the cell. The X-rays, diffracted by the sample, were measured by using 10 energy dispersive detectors. Only detectors 1, 5, 9, and 10 indicated, which are the detectors on which our analysis is based [after *Burnley and Zhang*, 2008].

then each grain will contribute a diffraction signal with different lattice spacings in the axial and transverse detectors. Any departure from this lattice spacing is therefore due to nonuniform or deviatoric local stress. If the stress field is not uniform, but varies from sample point to sample point, then each detector will collect scattering from a range of lattice spacings with a resulting peak broadening. Such heterogeneity must be due to local deviatoric stress. The stress on each grain can be characterized by the three principal stresses and the orientation of the stress tensor. Previous studies [*Weidner*, 1998; *Weidner et al.*, 1998] demonstrate that stress derived from the full width at half maximum (peak width measured at half of the maximum peak height) of the strain distribution, ε, by $E^*\varepsilon = \sigma_1 - \sigma_3$ is the differential stress experienced by roughly half of the grains, where E is the Young's modulus.

Lattice spacings were determined from the diffraction pattern via calibration spectra that were collected at the start of each experiment. The X-ray detectors are arranged to sample lattice spacing as a function of angle from the axial to the transverse direction. The position of the diffraction peak yields the centroid of lattice spacing of the particular reflection in the sample. The shape of the diffraction peak yields the distribution of lattice spacings of the particular reflection in the sample. Thus, this tool enables us to directly measure stress sensitive properties within the sample itself. The spectra are collected as the sample is compressed in a DIA press [*Durham et al.*, 2002; *Wang et al.*, 2003]. Each diffraction spectra was collected over a period of 100–500 s, with up to six positions sampled along the axial direction repeatedly as pressure was increased over a few hours. Here we focus on two of the experiments; one where the pressure reached 5 GPa (SIO2_53, International Geo Sample Numbers IGSN: IECEE0005) and a second that reached 5.6 GPa (SIO2_55, IGSN: IECEE0007). In other respects, these two experiments are almost identical to each other except that SIO2_55 spectra were collected over a longer time period of 500 s (Table 1). While we concentrate here on these two experiments, the results of all the other experiments were entirely consistent with these.

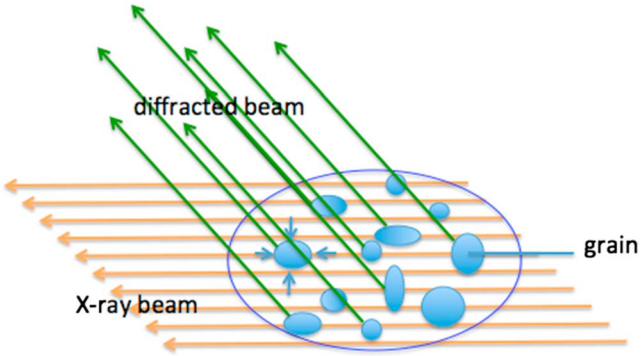

Figure 3. Each diffraction peak is the sum of diffraction from the relatively small number of grains within this volume that are appropriately oriented for diffraction. These grains share the characteristic that the normal to the particular diffraction plane (e.g., [101]) bisects the angle between the incident beam and the diffracted beam. Thus, the lattice spacing of each grain or portion of a grain samples the local stress field [after *Weidner*, 1998].

3. Results and Discussion

Energy dispersive X-ray diffraction data, generated during progressive compression of the quartz aggregate from 0 to 5.6 GPa, are plotted as intensity versus energy in Figure 4. While the [101] peak (identified as the second peak on the increasing energy axis, according to the International Center of Diffraction Data database: Joint Committee on Powder Diffraction Standards JCPDS-46-1045) has the highest intensity, all peaks broaden with pressure, indicating increasing deviatoric microstress with increasing pressure. The strong [101] peak is a signature of the quartz diffraction pattern due to its intensity and will therefore be the focus of the analysis below. The other peaks exhibit similar characteristics but with larger uncertainties. We now focus on the diffraction peaks in the transverse (detector 5) and axial (detector 9) directions, since they represent the extremes of behavior for all of the samples.

3.1. Lattice Spacing Analysis: Pressure Versus Macrostress

Lattice spacings ("d-spacings") were analyzed individually by using the Plot85 software program which utilizes a pseudo-Voigt auto peak fitting routine. "Goodness of fit" values were then used to determine if manual refitting would be required for more reliable results. We used the novaculite spectra to determine the pressure and the quartz aggregate spectra to define local sample macrostresses by using the elastic constants and lattice parameters from Table 2 [*Simmons and Wang*, 1971]. The volume of the unit cell ($V = \frac{1}{2} a^2 c$) was estimated by using the d-spacings from [101] and [112] peaks. The data for novaculite were then fitted to a third-order Birch-Murnaghan P-V equation of state to determine pressure, given the bulk modulus (κ_o) and its first pressure derivation ($\frac{\delta \kappa_o}{\delta P} = \kappa_o{}'$) from Table 2 [*Birch*, 1947; *Birch*, 1952].

Even though the sample is loaded in cubic symmetry, the solid-pressure medium used in the DIA apparatus may deliver a macroscopic deviatoric stress to the sample. Here we assume that the cylindrical symmetry of the cell assembly is the determining factor in producing this deviatoric stress, thereby creating a cylindrically symmetric stress field. The detector array allows us to determine the complete macrostress field for such a symmetry. If the field has cylindrical symmetry, then the difference in the d-spacing observed at $\psi = 0°$ and $\psi = 90°$ can be used as a measure of differential stress supported by the polycrystal [*Weidner et al.*, 1992]. Confirmation of the cylindrical symmetry comes from analysis of the d-spacing from all detectors. We use the methodology summarized in *Singh et al.* [1998] to calculate the magnitude of the differential stress. This method essentially associates the minimum d-spacing with the maximum principal stress. Using the known elastic constants and the measured elastic strain, we can then determine the stress.

In Figure 5a we show data on the volume compression of the solid grains within the quartz aggregate and the crystallites within the novaculite as a function of pressure. The key feature is that the volume compression of the grains within the quartz aggregate is significantly lower than that of the novaculite at pressures around 400 to 600 MPa and again between about 2.7 and 3.8 GPa. The divergence of the curves in the region of 400–600 MPa is observed consistently in all eight experiments. We interpret this as the pressure range where the quartz aggregate collapses, so that the pore space decreases, thus reducing the pressure in the aggregate and the stress on the solid grains. This is also the pressure range over which grain crushing and pore collapse are reported in the literature for porous sandstones [e.g., *Zhang et al.*, 1990]. Figure 5b illustrates the d-spacing for peak [101] as a function of pressure. The change in d-spacing of the quartz aggregate with pressure in the transverse direction is very similar to that of the novaculite. By contrast, the change in the d-spacing of the quartz aggregate in the axial direction is much lower than for the novaculite crystallites as a function of pressure. We therefore conclude that the direction of maximum collapse (compaction) is the axial direction. In essence, the solid parts of both materials compress with similar resistance in the transverse direction. In the axial direction, the solid parts of the quartz aggregate compress very little, compared with the crystallites in the novaculite. This can be explained by the large reduction of the pore space in the quartz aggregate due to pore collapse. This is evident by the lack of compression of the [101] lattice planes in the quartz aggregate in this orientation.

The volume compression anomaly between 2.7 and 3.8 GPa could be due to several possibilities. First, it could be due to a further collapse of pore space. As we see in the following section, this is strong evidence that significant pore space remains open throughout the pressure range explored in this study. The closure of that pore space could occur over a broad pressure range or over a small pressure range depending on the detailed mechanism of collapse. Second, it could be an artifact of the data analysis methodology. The

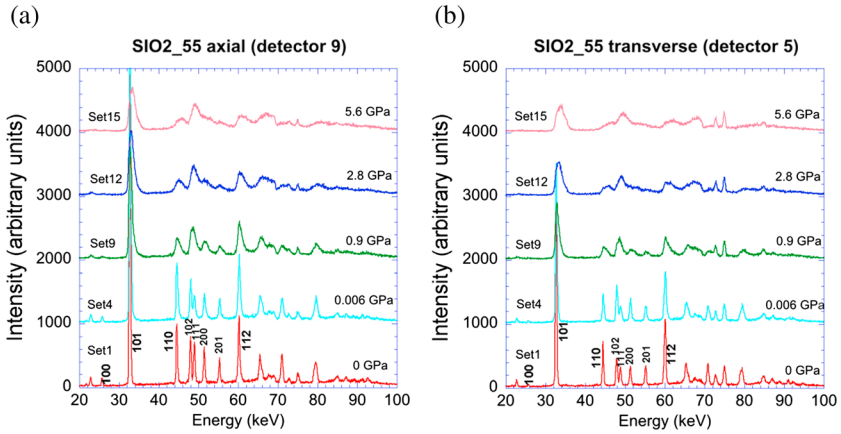

Figure 4. Energy dispersive X-ray diffraction data, generated during progressive compression of the solid grains within quartz aggregate (experiment SIO2_55) from 0 to 5.6 GPa, are plotted. The data are shown in the axial (Figure 4a) and transverse (Figure 4b) directions. The lattice planes are marked for the diffraction data at ambient pressure.

diffraction peaks broaden significantly over this pressure range, and the peak fitting model may be inadequate to identify properly the "average" lattice spacing for these peaks. These possibilities will be discussed in more detail following our analysis of peak broadening in the next section.

3.2. Full Width at Half Maximum of Diffraction Peaks: Microstress

In Figure 6 we illustrate a number of spectra for experiment SIO2_55. At room pressure, diffraction spectra from the quartz aggregate and the novaculite were essentially identical (experiment SIO2_55peak2-Set1 in Figure 6). The relative intensities of all the peaks, the positions of all the peaks, and the widths of all the peaks were virtually indistinguishable between the two materials. Under compression, as the pressure was increased, the peak width remained constant for the novaculite. By contrast, for the quartz aggregate the peak width broadened considerably with increasing pressure. In Figure 6, we plot the quartz aggregate peaks (both axial and transverse) at selected pressures against the novaculite peak at zero pressure, for ease of comparison. Furthermore, as the pressure is increased, the peak position shifts to higher energy for the centroid of the quartz aggregate peak (the novaculite peak also shifts to higher energy with increasing pressure, but this is not shown in this figure). Higher energy is equivalent to lower d-spacing but, for consistency, we refer to the low d-spacing edge of the peak as the high-energy or high-pressure side in the following discussion. At pressures beyond P = ~0.9 GPa (experiment SIO2_55peak2-Set9 in Figure 6), the quartz aggregate peak broadens significantly with increasing pressure on the high-energy side while barely changing on the low-energy side, giving rise to an asymmetric peak. Even at the highest pressures of P = ~5.6 GPa, the quartz aggregate peak was still broadening in both axial and transverse directions, with no sign of halting (experiment SIO2_55peak2-Set15 in Figure 6). Meanwhile, the novaculite peak retained a similar shape as that at zero pressure throughout (however, we only show the novaculite peak at zero pressure in Figure 6 for simplicity).

Table 2. The Voight and Reuss Bound of Elastic Constants and Elastic Compliances of Quartz (Reference Code: 62887) Aggregate at Ambient Temperature Used in Calculations [*Simmons and Wang*, 1971]

	Reuss	Voight	Voight-Reuss-Hill Average		
Young's modulus (**E**)	90.3 GPa	101.1 GPa	95.7 GPa		
Shear modulus (**G**)	41.7 GPa	48.5 GPa	45.1 GPa		
Poisson's ratio (V)	0.041	0.084	0.0625		
Bulk modulus (**K**)	36.1 GPa	36.7 GPa	36.4 GPa		
Compressibility (β)	272.3 GPa^{-1}	276.8 GPa^{-1}	274.6 GPa^{-1}		
Elastic Compliances	S_{11} 1.278 Mb^{-1}	S_{33} 0.972 Mb^{-1}	S_{44} 1.997 Mb^{-1}	S_{12} −0.181 Mb^{-1}	S_{13} −0.123 Mb^{-1}

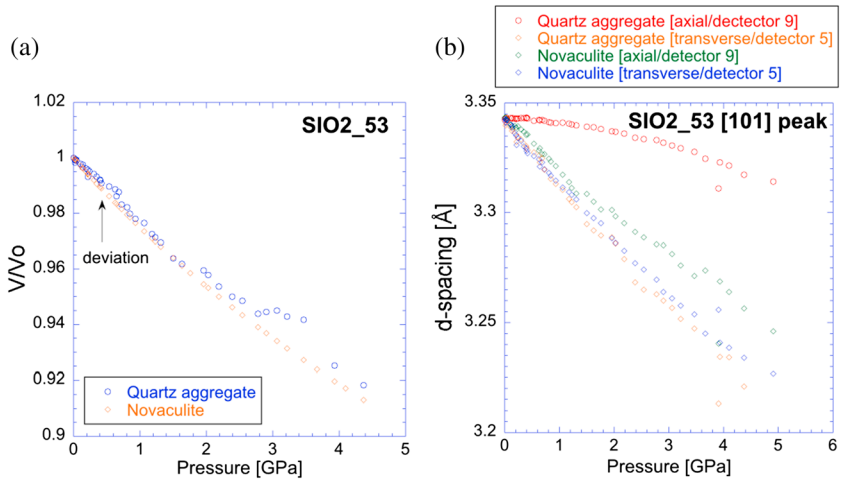

Figure 5. (a) Data for the volume compression of the solid grains within the quartz aggregate and the crystallites within the novaculite (experiment SIO2_53) as a function of pressure. (b) D-spacing for peak [101] as a function of pressure.

As the position of the diffraction peak indicates the distance between lattice planes, samples that contain grains with a distribution of lattice spacings will produce a diffraction peak that is broadened. The broadened peak is simply a convolution of the instrument response with the distribution of lattice spacings in the sample [*Lavina et al.*, 2014]. A distribution of lattice spacings implies a distribution of strain within the grains. This strain heterogeneity in the sample is produced by a stress heterogeneity, so we can use the broadening of the diffraction peaks to illuminate the microstress distribution in the sample [*Weidner*, 1998]. The only other major factor that can cause peak broadening is grain size reduction. However, a significant fraction of grains would need to be smaller than 100 nm in order to be detected by the energy dispersive detector [*Weidner*, 1998]. Furthermore, diffraction data collected after the pressure was released exhibited spectra with the same peak widths as the initial spectra collected at zero pressure. Hence, we consider that grain size reduction has not been an issue in these experiments.

The standard metric for estimating the microstress (differential stress) from diffraction data is the full width at half maximum (FWHM) of the diffraction peak. FWHM is the peak width measured at half of the maximum peak height. To further illustrate how we measure FWHM, a green horizontal line with two vertical lines that mark the FWHM upper and lower energy bounds is drawn for experiment SIO2_55peak2-Set1 in Figure 6. The FWHM is calculated by the difference of the energy bounds (i.e., ~ 0.4 keV). *Gerward et al.* [1976] demonstrated that for energy dispersive data, the total observed FWHM (W_o) is given by $W_o^2 = W_s^2 + W_d^2 + W_i^2$, where the subscript s refers to strain, d to grain size, and i to instrument. In other words, the total FWHM observable is composed of peak broadening due to strain (W_s), grain size (W_d), and the instrument (W_i). Since the peak broadening due to grain size (W_d) is below the detectable range (i.e., $W_d = 0$), we can estimate the broadening due to strain (W_s^2) from the observed FWHM (W_o^2) by subtracting the response due to instrumentation (W_i^2) (which can be obtained from the zero pressure spectra). If the broadening due to strain (W_s) is measured in Å (unit of length of lattice spacing), then strain is W_s/d, where d is the hydrostatic lattice spacing and the differential stress is given by E^*W_s/d, where E is the Young's modulus. If the stress distribution in the grains of the whole sample is Gaussian, then roughly half of the grains in the sample volume will be at a differential stress that exceeds this value [*Weidner*, 1998; *Weidner et al.*, 1998].

Figure 7 illustrates the differential stress, determined by using the peak broadening method (E^*W_s/d), for both the quartz aggregate and the novaculite as a function of pressure. While the values are based solely on the [101] peak, the other peaks yield similar and consistent values. As noted above, the novaculite peaks show little or no broadening and hence only an extremely low amount of differential stress. By contrast, the quartz aggregate exhibits a very high differential stress in both orientations. Furthermore, the differential stress in the transverse direction is about twice that in the axial direction and actually exceeds the applied pressure. This is consistent with the illustration in Figure 5 that the axial direction is supporting a significantly lower load than the transverse direction, given that the load is the driving force for the differential stress. The differential stress at the onset of pore collapse was about 1 GPa.

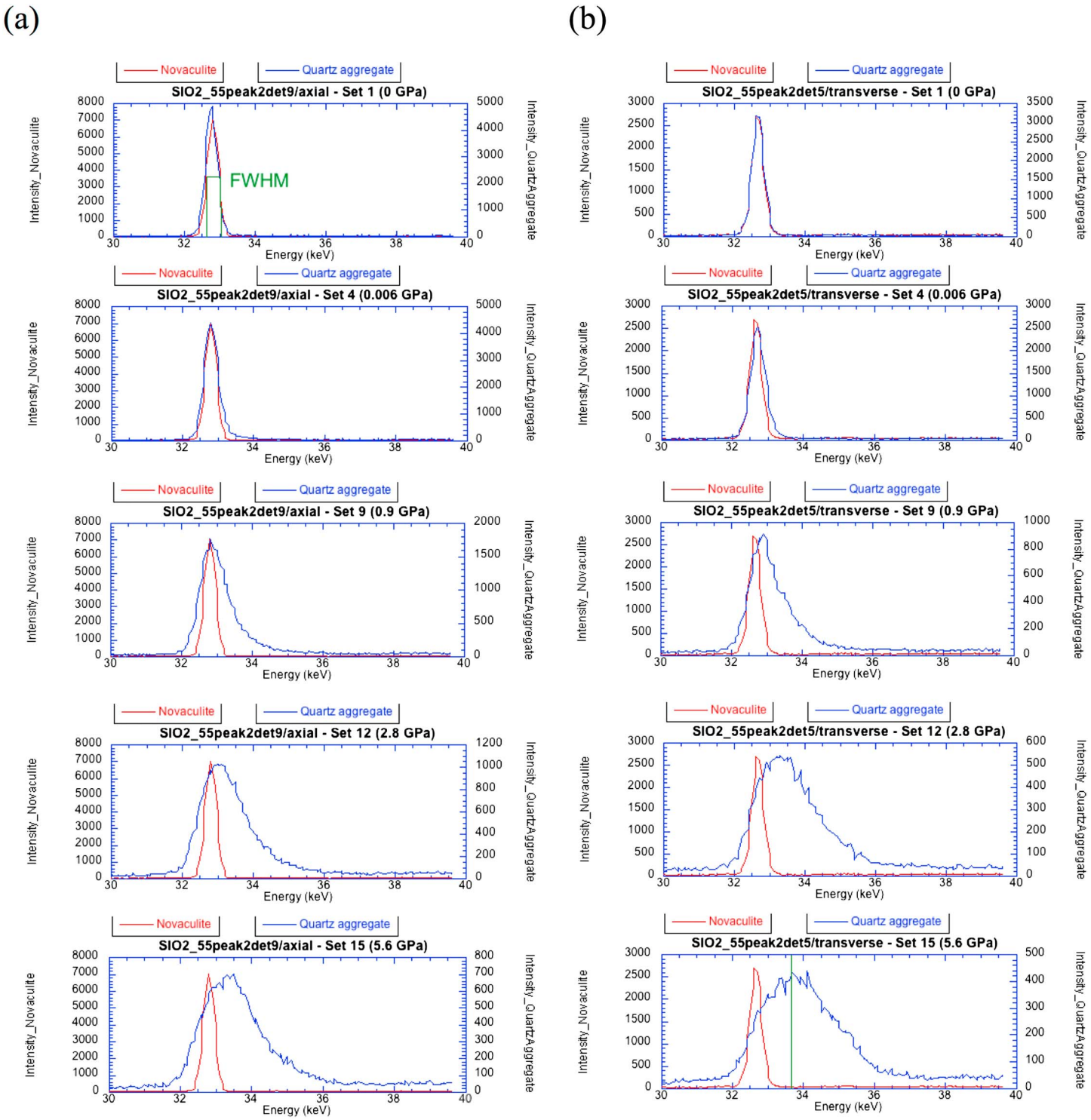

Figure 6. Evolution of the [101] peak for solid grains within quartz aggregate (blue) peaks at selected pressures against the crystallites within novaculite peak (red) at zero pressure. The data are shown in the *axial* (Figure 6a) and *transverse* (Figure 6b) direction under compression (experiment SIO2_55).

As noted earlier, the peaks broaden asymmetrically from relatively low pressure, and this becomes more significant at higher pressure. In fact, the evolution of the peak shape is very similar to that reported for cold compression of diamond powder [*Weidner et al.*, 1994]. Very strong granular materials are able to support high loads on some of the grains, while other grains support only relatively low loads, or at least support

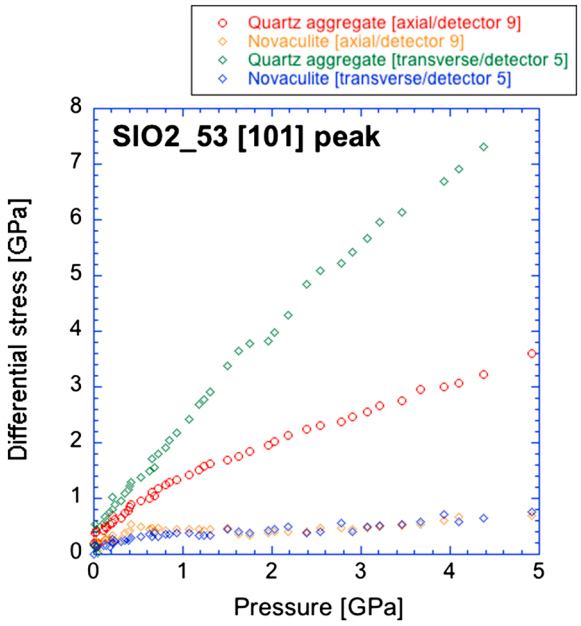

Figure 7. Differential stress, determined by using the peak broadening method (E^*W_s/d), for both the solid grains within quartz aggregate and the crystallites within novaculite (experiment SIO2_53) as a function of pressure.

low normal stresses in some directions. In particular, the [101] peak for the quartz aggregate is displayed for different applied pressures in comparison with the [101] peak for novaculite at zero pressure in Figure 6. A notable feature is that as the pressure is increased, the low-energy sides of both the axial and transverse quartz aggregate peaks shift by only a very small amount relative to the large shifts seen for the high-energy sides. This implies that there exists a significant population of grains that remain stress-free in both orientations. This can occur only if there remains a significant number of grains with at least a part of their surface area bounded by voids at zero pressure, even at the highest applied pressure.

Determination of the actual stress distribution requires a deconvolution of the instrument response from the observed peak. Here we use the ambient pressure peak as representative of the instrument response. We then find a distribution of peaks (delta functions) that can be convolved with the instrument to produce the shape of the observed peak by using a least squares fit as the criteria and applying this to selected peaks in the spectra. Figure 8 illustrates the result for the [101] peak. This process does not produce a unique solution in so much as the resolution is limited by the width of the instrument peak. However, this distribution of peak heights in the deconvoluted signal (plotted in red in Figure 8) represents the minimum sum of squares. The largest peak in the deconvoluted signal of the quartz aggregate is in the energy range of 33.35–33.45 keV. The results indicate that it was impossible to deconvolve the quartz aggregate signal without this largest peak. Using the novaculite peak at ambient pressure as a reference, the presence of this largest peak implies that most of the grains in the quartz aggregate are compressed at a value not higher than the ambient pressure. Hence, this also reinforces the suggestion that a significant number of grains have at least a part of their surface area bounded by voids at zero pressure.

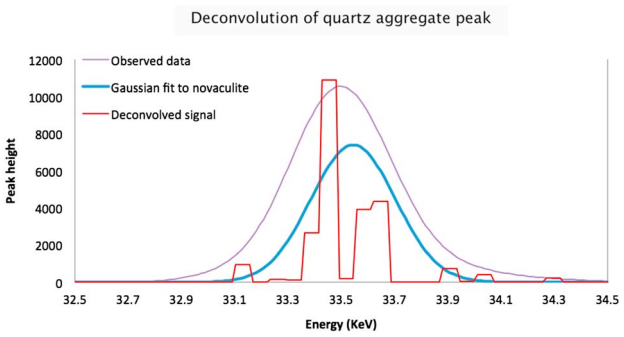

Figure 8. Result of deconvolution (red) of the observed [101] peak (purple) of the solid grains of quartz aggregate. The deconvolved signal shows that the distribution of peak heights with energy in the range of 32.5 keV to 34.5 keV. The Gaussian fit to the novaculite peak is plotted for comparison (blue).

3.3. Micromechanics of Quartz Aggregate Deformation

3.3.1. Microstructural Observations of Quartz Aggregate

Post-mortem microstructural observations of deformed samples can shed light on the deformation mechanisms and micromechanics of damage accumulation and failure. We prepared 10 thin sections from our deformed quartz aggregate samples. These were made by grinding them to 33 μm thickness, after impregnating them with blue-dyed epoxy resin to preserve their postmortem microstructure and aid the identification of pore space. The finished sections were first gold-coated

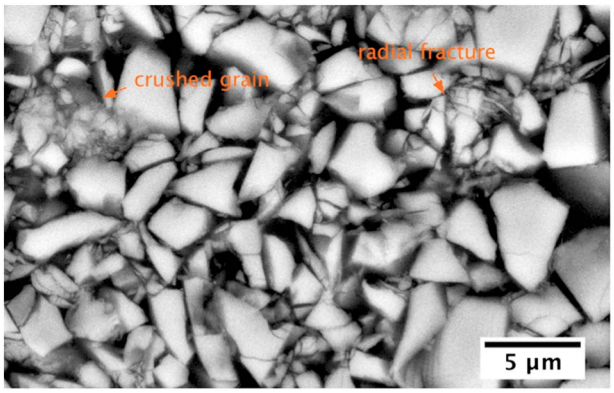

Figure 9. This figure which refers to a representative micrograph shows quartz grains from sample [SIO2_48] that had been deformed to a pressure of ~1.2 GPa. The deformed grains show that fractures radiate from grain-to-grain contacts. The cone-shaped fracture pattern initiated at the grain contact is reminiscent of tensile indentation fractures, commonly referred to as Hertzian fractures.

and then studied by using an LEO 1550 scanning electron microscope with a voltage of up to 20 kV.

Microstructural observations revealed that quartz grains were dominated by both transgranular cracks (cracks that extend across more than one grain) and intragranular cracks (cracks that stop within the boundary of a single grain) mostly induced at grain-to-grain contacts (terminology reviewed in *Scholle and Ulmer-Scholle* [2003]). A representative micrograph (Figure 9) shows quartz grains from sample [SIO2_48] that had been deformed to a pressure of ~1.2 GPa. The deformed grains show that fractures radiate from grain-to-grain contacts. The cone-shaped fracture pattern initiated at the grain contact is reminiscent of tensile indentation fractures, commonly referred to as Hertzian fractures [e.g., *Wilshaw*, 1971; *Gallagher et al.*, 1987; *Zhang et al.*, 1990]. All the other micrographs show similar features. Based on these microstructural observations, theoretical modeling of grain crushing known as Hertzian contact theory was employed for the following analysis.

3.3.2. Analysis of Hertzian Fracture in the Quartz Aggregate

Hertzian contact stress, first proposed and evaluated by Heinrich Hertz in 1882, was defined as the localized stress developed when two curved surfaces come into contact and are deformed under load. To evaluate the extent of deformation, the Hertzian contact theory is dependent on the elastic properties of two bodies, the radii of curvature of the surfaces and the normal contact force. This theory has since been applied to a wide variety of problems in contact mechanics including mechanics of rock and minerals. By assuming that both grains are isotropic and elastic, the solution can be simplified to the Hertzian elastic contact theory that provides an analytical model for the stress distribution in the vicinity of the contact. Since the contact area between grains is greatly reduced in a porous media, the stress will be greatly increased at the contact points. The maximum hoop stress will be located close to the circular external boundary of the contacting area, and the Hertzian model postulates that this extensional hoop stress is the seed of failure associated with crack nucleation and propagation. Hertzian fracture mechanics can therefore be used to estimate the onset of failure by grain crushing (P^*) in granular materials [e.g., *Wong et al.*, 2003]. P^* is defined as the "applied pressure" at which the sample transitions from elastic to inelastic compaction under hydrostatic loading. It is associated with a nonlinear decrease in porosity that is commonly accompanied by pore collapse, intense microcracking, and an associated surge in acoustic emission activity.

Using the relationship from *Wong et al.* [2003], and assuming a porosity of 25%, a mean grain radius of 2 μm, and P^* of 400 MPa, we calculate a contact stress of 6 GPa and an associated hoop stress of 5 GPa, or a differential stress of 11 GPa. This is in contrast to the measured 1 GPa. Figure 10 illustrates the [101] diffraction peak at 400 MPa with markers indicating the expected broadening for differential stresses of 1 GPa and 11 GPa. Clearly, the Hertzian model predicts a broadening that is much larger than observed. A lower stress intensification requires that the contact area is much greater than expected from spherical grains. In addition, the 1 GPa differential stress is much less than what is expected to fracture the quartz grains. Furthermore, the Hertzian model would predict that the differential stress will saturate at the stress level required to break the grains. In contrast, we observe the differential stress to continue to increase as P is raised above P^*. The Hertzian model would also predict that the collapse should be isotropic. Yet we observe the collapse to be very anisotropic as discussed above.

Despite the average stresses that we observed in this study being much higher than any we would expect to encounter under any reasonable reservoir conditions, we suggest that the ratio between the average stress

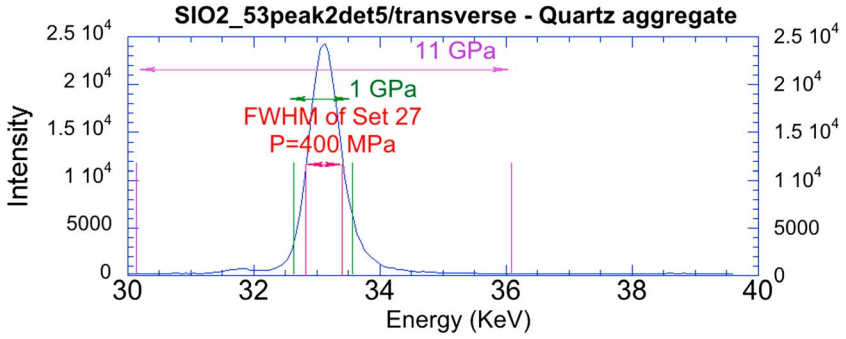

Figure 10. This figure shows the [101] diffraction peak of solid grains within quartz aggregate at 400 MPa (with red markers indicating its full width at half maximum in the range of ~32.8 to ~33.4 keV). The predicted peak widths are also drawn for differential stresses of 1 GPa (with green markers indicating the range of ~32.6 to ~33.5 keV) and 11 GPa (with purple markers indicating the range of ~30.1 to ~36.1 KeV), respectively.

calculated over the whole sample area and the local stress on the grain contacts is robust and will be applicable to scenarios at any stress level. Although the stresses required to produce compaction in the quartz aggregate under quasi-hydrostatic loading in our study is significantly higher than that likely to ever be encountered under normal reservoir conditions, we note that compaction is always enhanced in the presence of shear stresses (e.g., as reviewed in *Wong and Baud* [2012]). Under such shear-enhanced compaction, we would expect that compaction in quartz aggregates would occur at a significantly lower mean stress than P^*.

3.4. Conclusion

To conclude, this study of a quartz aggregate yields three features regarding the mechanics of compression. First, we observe an event that we associate with collapse that occurs at about 400–600 MPa, in agreement with the literature values. In this region, the sample compresses significantly with little increase in pressure. Second, at the time of collapse, the differential microscopic stress is about 1000 MPa. These values are about an order of magnitude lower than those predicted by a model based on Hertzian fracture mechanics. Third, we observe that the stress field in both axial and transverse direction has a dominant number of grains that remain at zero stress even though the mean stress is significantly large at 5.6 GPa. This implies that there remains a significant number of grains with at least a part of their surface area bounded by voids at zero pressure, even at the highest applied pressure.

Acknowledgments

The authors would like to acknowledge Richard Triplett (Stony Brook University) for the assistance in data acquisition, David Mann (High Mesa Petrographics) for thin section preparation, and Jim Quinn (Stony Brook University) for SEM imaging. The authors would also like to acknowledge Pamela Burnley (UNLV) for providing the novaculite samples. The authors are grateful to Przemyslaw Dera (University of Hawaii), Caleb Holyoke (University of Akron), Daniel Davis (Stony Brook University), Lars Ehm (Mineral Physics Institute), and Christiane Stidham (Stony Brook University) for useful discussion. The authors would also like to acknowledge Pamela Burnley and an anonymous reviewer for their helpful comments which improved the manuscript. This research was supported by COMPRES, the Consortium for Materials Properties Research in Earth Sciences under NSF cooperative agreement EAR 11-57758 and by the Mineral Physics Institute, Stony Brook University. The authors acknowledge NSF for research funding for this program through EAR 1361463, EAR 1045629, and EAR 1141895. All the data files are available from the authors upon request (scheung9@wisc.edu). The samples and data are achived at Mineral Physics Institute at Stony Brook University. The authors would like to acknowledge the use of the National Synchrotron Light Source, Brookhaven National Laboratory, supported by the U.S. Department of Energy, Office of Science, Office of Basic Energy Sciences, under contract DE-AC02-98CH10886. This research also used resources of the Advanced Photon Source, a U.S. Department of Energy (DOE) Office of Science User Facility operated for the DOE Office of Science by Argonne National Laboratory under contract DE-AC02-06CH11357.

References

Birch, F. (1947), Finite elastic strain of cubic crystals, *Phys. Rev.*, *71*(11), 809–824.

Birch, F. (1952), Elasticity and constitution of the Earth's interior, *J. Geophys. Res.*, *37*(2), 227–286.

Burnley, P. C., and D. Zhang (2008), Interpreting in situ X-ray diffraction data from high pressure deformation experiments using elastic–plastic self-consistent models: An example using quartz, *J. Phys. Condens. Matter*, *20*(28), 285,201.

Durham, W. B., D. J. Weidner, and S. Karato (2002), New deevelopments in deformation experiments at high pressure, *Rev. Mineral. Geochem.*, *51*(1), 21–49, doi:10.2138/gsrmg.51.1.21.

Gallagher, J. J. (1987), Fractography of sand grains broken by uniaxial compression, in *Clastic Particles: Scanning Electron Microscopy and Shape Analysis of Sedimentary and Volcanic Clasts*, edited by J. R. Marshall, pp. 189–228, Van Nostrand Reinhold Co., New York.

Gerward, L., S. Mo, and H. Topso (1976), Particle size and strain broadening in energy-dispersive X-ray powder patterns, *J. Appl. Phys.*, *47*(3), 822–825.

Lavina, B., P. Dera, and R. T. Downs (2014), Modern X-ray diffraction methods in mineralogy and geosciences, *Rev. Mineral. Geochem.*, *78*(1), 1–31, doi:10.2138/rmg.2014.78.1.

Peng, S. D. (1971), Stresses within elastic circular cylinders loaded uniaxially and triaxially, *Int. J. Rock Mech. Min. Sci. Geomech. Abstr.*, *8*(5), 399–432, doi:10.1016/1365-1609(71)90009-8.

Scholle, P. A., and D. S. Ulmer-Scholle (2003), A color guide to the petrography of carbonate rocks: Grains, textures, porosity, diagenesis, *AAPG Mem.*, *77*.

Simmons, G., and H. Wang (1971), *Single Crystal Elastic Constants and Calculated Aggregate Properties*, pp. 135–160, MIT Press, Cambridge.

Singh, A. K., C. Balasingh, and H. Mao (1998), Analysis of lattice strains measured under nonhydrostatic pressure, *J. Appl. Phys.*, *83*(12), 7567, doi:10.1063/1.367872.

Terzaghi, K. (1923), Die berechnung der durchlassigkeitsziffer des tones aus dem verlauf der hydrodynamischen spannungserscheinungen, *Sitzungsber. Akad. Wiss. Wien, Math.-Naturwiss. Kl., Abt. IIa*, *132*, 125–138.

Wang, Y., W. B. Durham, I. C. Getting, and D. J. Weidner (2003), The deformation-DIA: A new apparatus for high temperature triaxial deformation to pressures up to 15 GPa, *Rev. Sci. Instrum.*, *74*(6), 3002–3011.

Weidner, D. J., M. T. Vaughan, J. Ko, Y. Wang, X. Liu, A. Yeganeh Haeri, R. E. Pacalo, and Y. Zhao (1992), *Characterization of Stress, Pressure, and Temperature in SAm85, a DIA Type High Pressure Apparatus*, *Geophys. Monogr. Ser.*, pp. 13–17, AGU, Washington, D. C.
Weidner, D. J., Y. Wang, and M. T. Vaughan (1994), Strength of diamond, *Science*, *266*(5184), 419–422.
Weidner, D. J. (1998), Rheological studies at high pressure, *Rev. Mineral. Geochem.*, *37*(1), 493–524.
Weidner, D. J., Y. Wang, G. Chen, J. Ando, and M. T. Vaughan (1998), Rheology measurements at high pressure and temperature, in *Properties of Earth and Planetary Materials at High Pressure and Temperature*, edited by M. H. Manghnani and T. Yagi, pp. 473–482, AGU, Washington, D. C., doi:10.1029/GM101p0473.
Wilshaw, T. R. (1971), The Hertzian fracture test, *J. Phys. D: Appl. Phys.*, *4*(10), 1567–1581, doi:10.1088/0022-3727/4/10/316.
Wong, T. F., C. David, and B. Menendez (2003), Mechanical compaction, *Int. Geophys. Ser.*, *89*, 55–114.
Wong, T.-F., and P. Baud (2012), The brittle-ductile transition in porous rock: A review, *J. Struct. Geol.*, *44*(C), 25–53, doi:10.1016/j.jsg.2012.07.010.
Zhang, J., T.-F. Wong, and D. M. Davis (1990), Micromechanics of pressure-induced grain crushing in porous rocks, *J. Geophys. Res.*, *95*(B1), 341, doi:10.1029/JB095ib01p00341.